

Article

Distinctive Effects of Surface Roughness and Ions Release on the Bacterial Adhesion and Inactivation of Textured Copper Oxide Surfaces

Akram Alhussein ^{1,*}, Lyliya Aouchiche ², Abdelhamid Hmima ³, Delphine Retraint ⁴ and Sami Rtimi ^{5,6,*}

¹ UR LASMIS, University of Technology of Troyes, Technological Pole of South Champagne, 26 Lavoisier rd, 52800 Nogent, France

² LEC2M, Mouloud Mammeri University of Tizi-Ouzou, Tizi-Ouzou 15000, Algeria

³ L2n, CNRS ERL 7004, University of Technology of Troyes, 12 Marie Curie rd, CS 42060, 10004 Troyes, France

⁴ UR LASMIS, University of Technology of Troyes, 12 Marie Curie rd, CS 42060, 10004 Troyes, France

⁵ Ecole Polytechnique Fédérale de Lausanne (EPFL), 1015 Lausanne, Switzerland

⁶ Global Institute for Water, Environment and Health (GIWEH), 1210 Geneva, Switzerland

* Correspondence: akram.alhussein@utt.fr (A.A.); rtimi.sami@gmail.com (S.R.)

Abstract: In this manuscript, we studied the effect of additive manufacturing pretreatment on bacterial adhesion and inactivation on copper-based interfaces. Sandblasting, mirror polishing and Surface Mechanical Attrition Treatment (SMAT) at high or low energies have been employed to modify the substrate's (316L stainless steel) roughness. The pretreated substrates were coated with thin copper films using magnetron sputtering. The thin copper films' composition and antibacterial activities were first optimized by being deposited on an Si wafer. We showed that the surface roughness profile influenced bacterial adhesion in the dark. Bacterial inactivation was monitored under indoor light. Stereomicroscopy imaging showed live/dead bacterial cells on the coated substrates. Scanning electron microscopy (SEM) showed homogeneous coating growths of copper with a columnar texture. The chemical composition of the deposited Cu thin films was carried out by Energy Dispersive X-ray Spectroscopy (EDX) and showed a uniform distribution of copper and oxygen, revealing the formation of copper oxides (Cu_xO). The oxygen content of the sputtered films varied from 7.8 to 25%, justifying the semi-conductor behavior of the thin films under indoor light. The crystallographic structure of the sputtered thin films was investigated using X-ray diffraction (XRD), showing the cubic Cu peaks and characteristic peaks of Cu₂O. The Cu peaks at 2θ values of 43.28°, 50.40° and 74.81° were attributed to the (111), (200) and (220) planes, respectively. The use of genetically modified bacteria (without porins) allowed the rationalization of the predominant effect of the extracellular bacterial inactivation compared to that of intracellular bacterial inactivation through ion release and diffusion.

Keywords: copper oxide; additive manufacturing; thin film; surface roughness; surface mechanical attrition treatment; bacterial inactivation



Citation: Alhussein, A.; Aouchiche, L.; Hmima, A.; Retraint, D.; Rtimi, S. Distinctive Effects of Surface Roughness and Ions Release on the Bacterial Adhesion and Inactivation of Textured Copper Oxide Surfaces. *Coatings* **2023**, *13*, 454. <https://doi.org/10.3390/coatings13020454>

Academic Editor: Joaquim Carneiro

Received: 16 January 2023

Revised: 31 January 2023

Accepted: 10 February 2023

Published: 16 February 2023



Copyright: © 2023 by the authors. Licensee MDPI, Basel, Switzerland. This article is an open access article distributed under the terms and conditions of the Creative Commons Attribution (CC BY) license (<https://creativecommons.org/licenses/by/4.0/>).

1. Introduction

During the last few years, the number of microbial infections has risen drastically. Many germs have developed a resistance to a large spectrum of antibiotics and have become stronger than ever. These germs are present in water/wastewater, indoor environments, and fomites [1–4]. Many approaches have been used to fight infections in the indoor environment such as spraying, detergents, ventilation, etc. Most of these technologies are curative. Today, there is a huge need for preventive technologies to fight microbial infections, especially in hospitals, transport, schools, workplaces settings, etc. [5,6].

Microorganisms such as bacteria and viruses commonly infect humans in the living environment. Several inorganic materials such as copper, zinc, and titanium dioxide have

been used as antimicrobial agents for decades. However, what is delaying their industrial implementation is their stability and their potential side effects or toxicity [5].

Recently, during the SARS-CoV-19 pandemic, many scientists stressed the antimicrobial uses of copper and copper oxides for hospital setting disinfection [7,8]. Cu ions are well known for their widespread antibacterial activities [6,9]. Copper oxides have been used for decades as antimicrobial agents [10–12]. The atomic structure of copper consists of filled electronic orbitals hopping around the positively charged nucleus. Copper oxide with concentrations in the ppm/ppb ranges was reported to induce the pathogens' cytotoxicity, leading to their death [11,12]. The antibacterial activity of copper oxides was reported to happen through (i) photo-generated reactive oxygen species (ROS) at the interface of the Cu semiconductors under appropriate light irradiation and (ii) ion diffusion to the intracellular compartment, leading to a metabolic disorder and cell death. Cuprous atoms strongly bind to thiol groups (–SH) mainly made of cysteine-forming steady S\Cu bonds with thiol-containing compounds with a high stability constant, reaching 10^{10} M^{-1} [13]. The functions of many enzymes inside bacterial cells are therefore inhibited by the ability of Cu ions to substitute essential ions such as Na, K, Zn, and Mg. Moreover, once copper ions enter a cell, they can generate reactive oxygen species (ROS) [14], produce phosphate hydrolysis and/or intercalate between base pairs, leading them to break off the hydrogen bonds responsible for DNA double-stranded conformation [15,16].

To preclude/decrease viral, fungal and antibiotic-resistant bacteria, lots of interest in solid inorganic nanocrystalline heterostructures is drawing attention [1,4,6]. Surface physical attributes may provide a more persistent form of inhibiting bacterial adhesion [17]. Combining chemical and physical surface characteristics can effectively hamper microbial invasion and growth (leading to biofilms). This is a bio-inspired way to reduce bacterial/viral adhesion and dissemination on hospital surfaces [18]. Mussels, sharks, crabs and skates possess antifouling properties at their most outer surface microscopic ridges and grooves. This is due to the surface roughness and the proteins and polysaccharides at the interface [18,19].

In this study, we combine the chemistry of the copper oxide thin film with the physical roughness of the substrate to study the adhesion and the disinfection of bacteria at the interface. Copper oxide thin films were deposited on stainless steel, often used in food processing and in producing pharmaceutical equipment, medical devices and door handles. The substrates were treated by mirror polishing (from now on, known as "P"), sandblasting ("S"), a low-energy Surface Mechanical Attrition Treatment (from now on, known as "Low SMAT") and a high-energy SMAT ("High SMAT").

In this work, we aim to show the effect of surface roughness on bacterial adhesion and inactivation at the interface of a catalytic surface. When working with bio-functional surfaces, the tribological characteristics are used to visualize the distribution of peaks and valleys that can affect the cells' adhesion. To differentiate the contribution of the surface roughness effect from that of the surface chemistry effect, porins-free bacteria have been used. These genetically modified microorganisms do not allow the penetration of copper ions into the intracellular compartment. This study is a step further in designing novel coated surfaces for indoor environments and/or food processing with the capability to hinder microbial adhesion and growth.

2. Experimental

2.1. Deposition of Copper Oxide Coatings

Copper oxide thin films were deposited on glass, silicon wafers and 316 L stainless steel substrates at room temperature by DC magnetron sputtering. Five thin films with different thicknesses and compositions were used. The surface of one face of the 316 L disc substrates (Φ 25 mm \times 8 mm thick) was mechanically treated to modify its roughness. The four following configurations were made: mirror polishing (P), sandblasting (S), low-energy SMAT (Low SMAT) and high-energy SMAT (High SMAT), where SMAT is the Surface Mechanical Attrition Treatment.

A pure Cu circular target (99.99% purity, 200 mm × 6 mm) was used. The chamber was evacuated to reach a pressure of 8×10^{-4} Pa. The distance between the copper target and the sample was fixed at 14 cm. Before deposition, the stainless-steel samples were cleaned by ultrasound path with acetone during 10 min, and then with ethanol for 8 min to remove all of the dirtiness caused by the handling. The substrates and Cu-target were cleaned for 15 min using Ar⁺ ions to remove the surface contaminants. The used bias voltage, Cu discharge current, Ar flow rate and sputtering chamber pressure were kept constant at 200 W, 1 A, 100 sccm and 0.37 Pa, respectively. After initial optimization, the thin films were deposited under a mixed atmosphere of Ar and O₂. All of the films were deposited with a constant flow rate of argon of 100 sccm and with a varying oxygen rate injected inside the chamber between 2 and 10 sccm. The different deposition times varied between 25 and 60 min to obtain films with different thicknesses (0.85–2.2 μm).

The sample holder rotation speed was set at 10 rpm and the working pressure was kept at 0.37 Pa. The thin films were deposited by applying a constant discharge current of 2 A to the Cu target. Table 1 presents the deposition parameters, chemical composition and thicknesses of the copper oxide coatings. After optimizing the thin film that leads to the fastest bacterial inactivation kinetics, this composition has been kept for pretreated substrates using low-energy SMAT, high-energy SMAT, mirror polishing, and sandblasting.

Table 1. Deposition parameters, thickness and chemical composition of Cu_xO coatings.

Coating N°	Gas Flow Rate (sccm)		Deposition Time (min)	Cu Target		Composition (at.%)		Film Thickness (μm)
	Ar	O ₂		I (A)	P (W)	O	Cu	
1		5	25					0.86
2		5	40		609	16.5	83.5	1.38
3	100	5	60	2				2.2
4		10	35		646	25.8	74.2	1.34
5		2	40		587	7.8	92.2	1.28

2.2. Characterization of the Samples by SEM, EDX, XRD and Profilometry

The film thickness and surface roughness were measured using an Altisurf 500 profilometer (ALTIMET, France). This device was equipped with a non-contact sensor, and the measurement accuracy was 20–22 nm.

The chemical composition of the deposited films was obtained by Energy Dispersive X-ray Spectroscopy (EDX) and quantified by Quantax Esprit software [20]. For each sample, the measurement was carried out on multiple zones of the sample. The elemental spectra and maps were acquired from SEM images by applying a high accelerating voltage of 15 kV and a pressure vacuum of 10^{-4} Pa, considering: a 60 kcps count mode, a 40 keV acquisition range and a 2 kcps initial counting rate. The coating cross-section images were obtained using a Hitachi SU8030 scanning electron microscope (SEM).

The crystallographic structure of the film was investigated by X-ray diffraction technique (XRD) by means of a Bruker AXS D8-Advance diffractometer equipped with Cu Kα radiation line ($\lambda_{Cu} = 0.15418$ nm).

2.3. Bacterial Adhesion and Inactivation under Indoor Light

Escherichia coli (*E. coli* K12) bacterium was obtained from the Deutsche Sammlung von Mikro-organismen und Zellkulturen GmbH (DSMZ), Braunschweig, Germany. Every sample was placed into a glass Petri dish, then inoculated with bacteria. The 100 μL culture aliquots with an initial concentration of 3.2×10^6 colony-forming unit per milliliter (CFU mL⁻¹) in NaCl/KCl were placed on the coated and uncoated (control) samples. After the preselected times, the samples were transferred into a sterile tube containing 900 μL autoclaved NaCl/KCl saline solution. This solution was subsequently mixed thoroughly

using a Vortex for 2 min. Serial dilutions were made in NaCl/KCl solution. A 100 μ L sample of each dilution was pipetted onto a nutrient agar plate, and then spread over the surface of the plate using the standard plate method. Agar plates were incubated with the lid down to prevent evaporation for 24 h before the colonies were counted. All experiments were carried out in triplicates and statistical analyses show standard deviation error bars (\pm SD, $n = 5\%$). All the used solutions and samples were autoclaved before use at 121 $^{\circ}$ C. The irradiation of the *E. coli* on the Cu-sputtered samples was carried out using Philips Master TLD-18 W/865 actinic lamps as used in hospital facilities, with an emission between 360 and 720 nm and with a light dose of 5 mW/cm². Control glass samples were cleaned ultrasonically in acetone for 15 min, rinsed in ethanol, and then dried with hot air.

The adhesion of the *E. coli* on the coated surfaces (with different roughness values) was carried out by immersing the samples into a 25 mL suspension of *E. coli* cells of a concentration of 3×10^6 CFU/mL. The recipient containing the sample and the bacterial suspension was then shaken gently at 37 $^{\circ}$ C for 10 min in the dark [17,21,22]. The non-adhered bacteria in the samples were removed by washing the surface with a phosphate-buffered solution (pH 7.2). The number of viable cells was determined after separating the adhered *E. coli* cells by ultra-sonication (50 W). Bacterial adhesion experiments were carried out in the dark to avoid the photocatalytic action of the copper oxide.

2.4. Genetically Modified Bacteria at the Interface of the Prepared Coating: Adhesion and Inactivation Kinetics

Genetically modified *E. coli* mutant strains deficient in porins were prepared according to protocols previously reported [23,24]. Table 2 shows the used genetically modified bacteria. Working with these modified bacteria allowed us to compare the bacterial inactivation kinetics induced by: (i) the ions able to penetrate inside the cell or (ii) by contact of the bacteria with the coated/sputtered surface (from now on, known as surface contact). The genetically modified porin-less *E. coli* TK 821 is isogenic with the K12 ATCC bacterial strain. Both bacteria contain genotypes that reproduce indefinitely and remain similar for many generations. The culture conditions used for the *E. coli* and the genetically modified *E. coli* were identical to limit the differences in the growth of both strains. The main porins proteins for *E. coli* membrane are OmpF and OmpC, which allow hydrophilic molecules to diffuse passively to the intracellular medium. OmpF is expressed preferentially in a low-osmotic-pressure medium, contrary to AmpC, which expresses in high osmolarity. The transcription of OmpF and OmpC requires the presence of the OmpR functional protein. However, in vitro, OmpR controls only the expression of OmpF, while OmpC is independent of OmpR [25].

Table 2. The used genetically modified *E. coli* strains used in this study.

Germ	Porins Specification
<i>E. coli</i> K-12 strain MC4100	<i>ompR</i> ⁺ , <i>ompF</i> ⁺ , <i>ompC</i> ⁺
<i>E. coli</i> MH1471	<i>ompR</i> ⁺ <i>ompF</i> ⁻ <i>ompC</i> ⁺
<i>E. coli</i> MH225	<i>ompR</i> ⁺ <i>ompF</i> ⁺ <i>ompC</i> ⁻
<i>E. coli</i> TK821	<i>ompR</i> ⁺ <i>ompF</i> ⁻ <i>ompC</i> ⁻

The different Omp gene combinations will allow us to understand the bacterial response to dissolved copper ions in different conditions. This will allow us to draw clear conclusions about the contribution of the intracellular effect of copper ions released from the sputtered surfaces presenting different roughness properties.

2.5. Live/Dead Cells at the Interface of the Prepared Coatings

Stereomicroscopy imaging was carried out on the samples inoculated with 10^8 CFU of *E. coli* and incubated for 2 h in a humidification chamber [26]. This method uses a fluorochrome-based staining procedure from Filmtracer™ LIVE/DEAD® Biofilm Viability Kit (Molecular Probes, Invitrogen). The kit contains a combination of the SYTO9® green fluorescent nucleic acid stain and propidium iodide (PI) fluorochromes for the staining of the live and dead cells, respectively. The sample fluorescence was monitored using a stereomicroscope (Leica MZ16 FA, Leica Microsystems GmbH Wetzlar, Germany). The images were processed using the LAS v.1.7.0 build 1240 software from Leica Microsystems CMS GmbH. Adhesion of bacteria at the interface of the coated samples was allowed for 5 min before washing the sample with sterile Milli-Q water to remove the non-adherent bacteria.

2.6. Ions Release from SMAT Prepared Surfaces

Copper ions release was determined by inductively coupled plasma mass spectrometry. The sample preparation and ion quantification have been previously detailed [25]. To better understand the contribution of copper atoms in bacterial inactivation, we performed an assumption to convert the total ionic copper quantified by ICP-MS into the molar copper content. This will give us an approximative magnitude of the copper atoms inactivating the bacteria from the intracellular compartment.

3. Results and Discussion

3.1. Analysis of the Surface Roughness after Pretreatment

The roughness of the 316 L substrates, which were mechanically treated according to different conditions, was measured and analyzed using an Altisurf 500 profilometer. Figure 1 shows the surface visualization and roughness profiles (see Figure S1). The Abbott–Firestone curves give a clear idea that is not visible with conventional roughness parameters. These graphs allow the generation of an average curve due to the nature of the distribution of the peaks and valleys of the treated surfaces in our case. Abbott–Firestone curves obey the American Society of Mechanical Engineering guidance (ASME B46.1) and the ISO 13565-2.

The mean values of surface roughness presented in Tables 3 and 4 were extracted from the profilometry images. The polished samples present the smoothest surface, and the sandblasted ones showed the highest roughness values.

Table 3. Average roughness of reference samples (substrates before film deposition).

Sample	Polished	Low-Energy SMAT	High-Energy SMAT	Sandblasted
Rk (μm)	0.21	0.55	0.34	4.75

Table 4. Arithmetic mean difference (Sa) and total height (St) of the surface of samples.

Sample	Polished	Low-Energy SMAT	High-Energy SMAT	Sandblasted
Sa (μm)	0.78	1.34	1.66	10.33
St (μm)	19.10	22.79	17.81	98.69

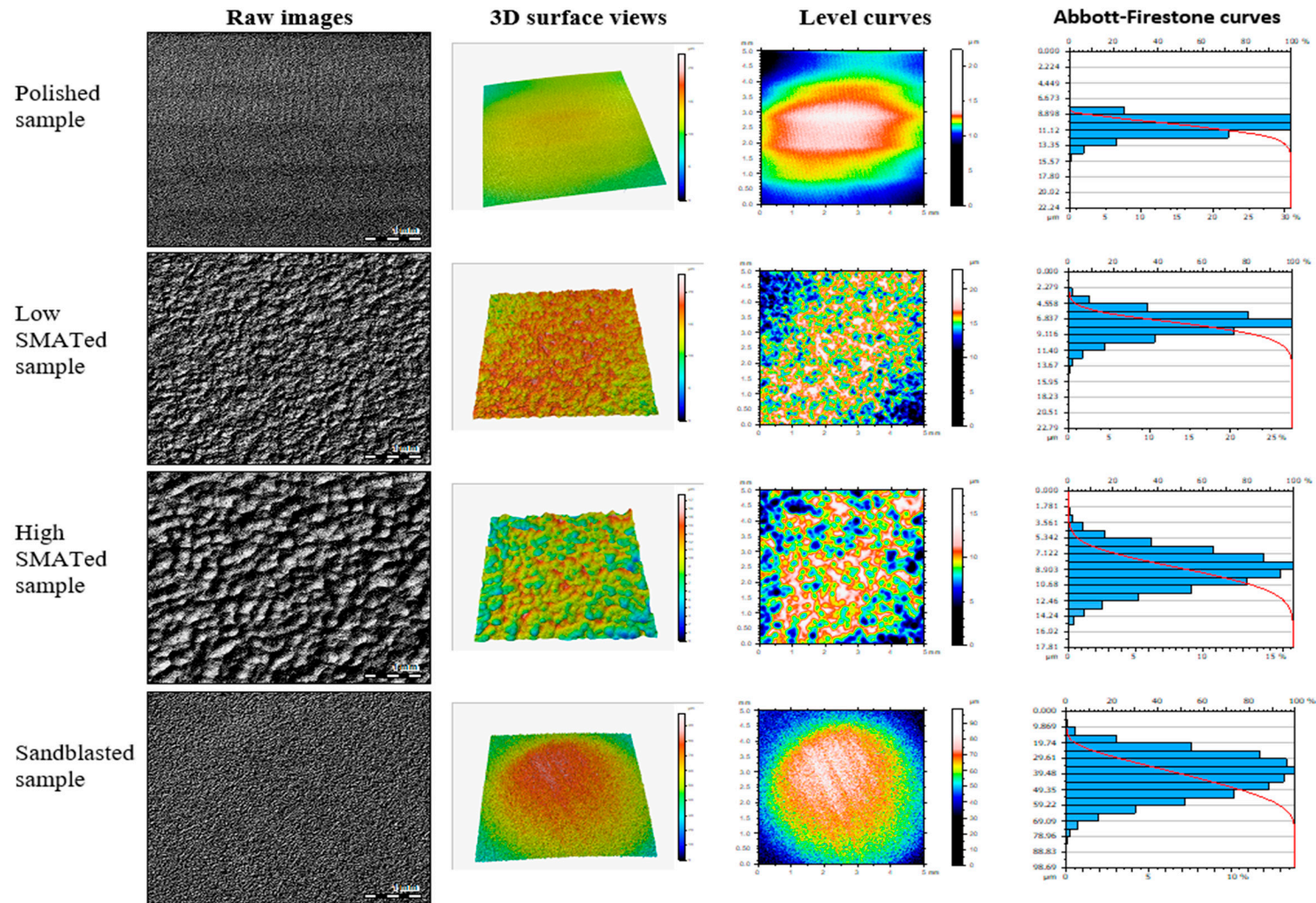


Figure 1. Profilometry characterization of the prepared 316 L substrates.

3.2. Microstructure, Crystallinity, Antibacterial Activity and Chemical Composition of the Prepared Thin Films

The cross-section and morphology of the prepared thin films are presented in Figure 2. The cross-section images show a columnar growth of the thin films. The deposition parameters were kept constant, particularly the sample holder rotation and the working pressure, which allowed us to obtain similar homogeneous coatings growth. Copper and oxygen are well distributed, and the columnar growth is well pronounced, as shown in Figure 2.

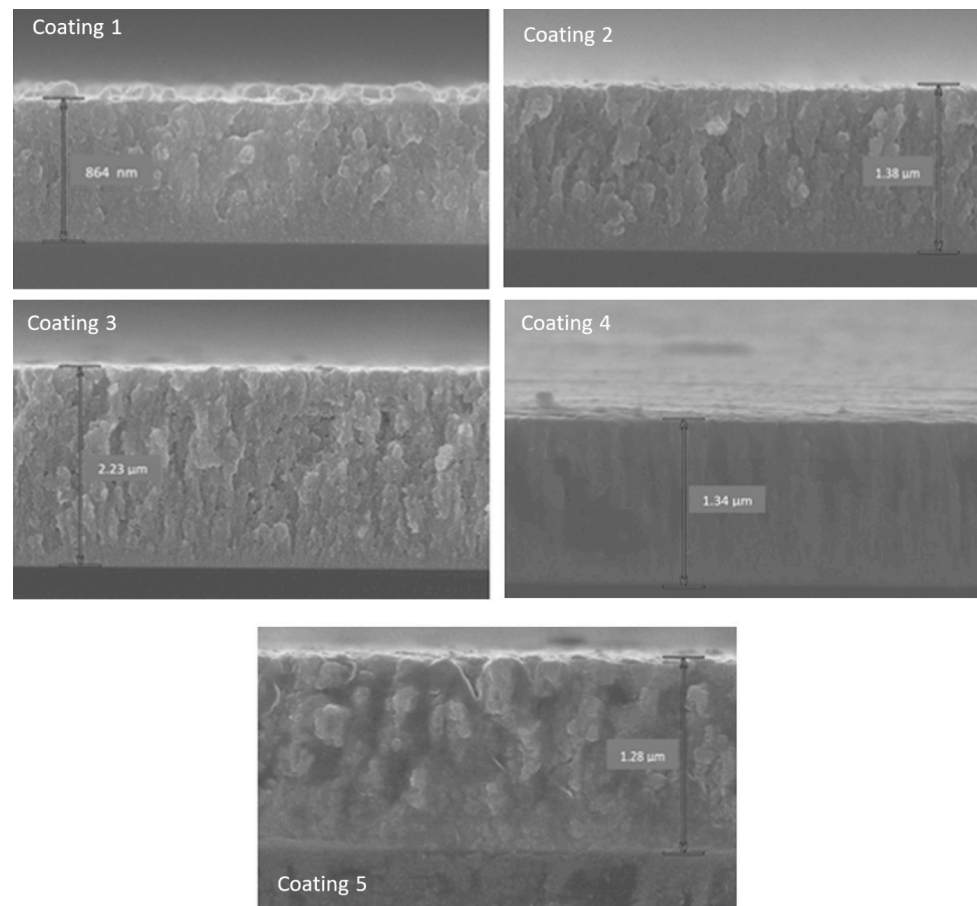


Figure 2. SEM cross-section images of copper oxide films.

The crystallinity of the prepared thin films was carried out using the XRD technique. Figure 3 presents the diffractograms of the five sputtered thin films. The films present peaks at the same scattering angles (2θ) corresponding to copper and copper oxide (Cu_2O). The Cu peaks at 2θ values of 43.28° , 50.40° and 74.81° correspond to the (111), (200) and (220) planes, respectively. The Cu_2O peak at 2θ value of 36.4° corresponds to the (111) plane. All diffraction peaks agree with the standard patterns for the pure face-centered cubic phase of copper (JCPDS No. 040836 and COD-4313211) and Cu_2O (JCPDS No. 050667 and COD-1010941). The peaks also present quasi-similar intensities, reflecting that the adopted preparation methods did not affect the crystalline structures of the five sputtered coatings, although the oxygen contents differed. Thus, the atomic arrangement of the sputtered thin layers and the interatomic distances led to a similar number of scatters per unit area of the atomic plane present in these thin layers [27]. The crystallite size was calculated considering the Cu (111) peak at the 2θ value of 43.28° presenting the highest intensity and the main crystalline phase. Table 5 shows the crystallite size from the different sputtered thin films.

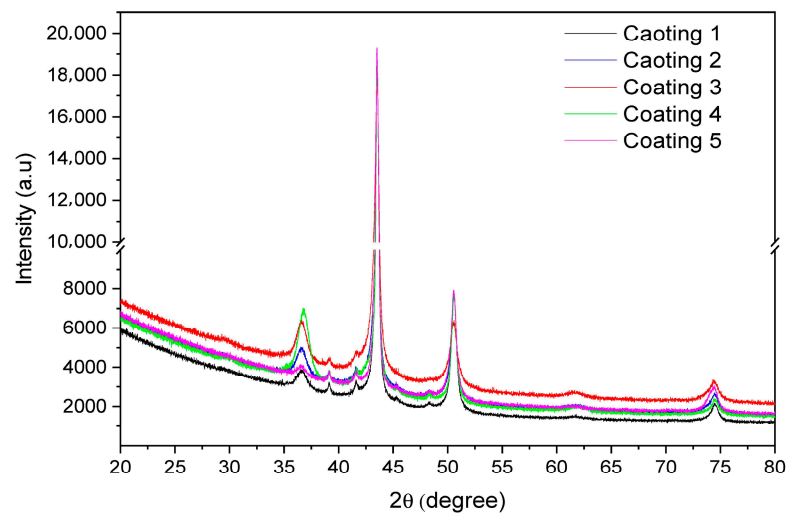


Figure 3. XRD diffractograms of Cu_xO thin films deposited on Si wafer.

Table 5. Crystallite sizes of the deposited copper oxide thin films.

Coating N°	Composition (at.%)		Film Thickness (μm)	Crystallite Size (nm)
	O	Cu		
1			0.86	26.1
2	16.5	83.5	1.38	24.3
3			2.2	17.7
4	25.8	74.2	1.34	26.4
5	7.8	92.2	1.28	24.3

It is readily seen from Tables 1 and 5 that the crystallite sizes are in the range 17.7–26.4 nm, and that increasing the oxygen flow rate up to 10 sccm led to an increase in the crystallite size from 24.3 to 26.4 nm. This latter observation is generally due to the decrease in the ion bombardment energy and the contamination of the Cu target by oxygen. Likewise, increasing the film thickness resulted in a grain refinement from 26.1 to 17.7 nm.

Furthermore, these results reflect the high reactivity of the sputtered copper ions toward oxygen in the magnetron chamber. Chandra et al. [28] reported the oxidation of copper during the deposition with an external oxygen source in the magnetron chamber, leading to the formation of Cu_2O . Kiwi and Rtimi [29] attributed the oxidation of copper in the magnetron chamber to the residual water monolayer remaining after the pre-pumped high vacuum before the sputtering process of copper.

J. Su et al. [30] calculated the contribution of residual oxygen in the oxidation of sputtered copper thin layers. They concluded that the O_2 source during high-pressure sputtering originated from the impurity of the inert gas (Ar gas 99.999 wt.%) rather than the residual O_2 in the pre-pumped high vacuum. Su et al. assumed the volume fraction of oxygen in the high vacuum to be close to the composition of air (21%), which we think was very high compared to the O_2 fraction inside the magnetron chamber as quantified by mass spectrometry that was recently reported for copper and silver [24].

The bacterial inactivation efficiency was tested for the five prepared coatings. Figure 4 shows that fast bacterial inactivation was obtained using coating 4. As seen in Table 1, this film was prepared using the highest oxygen amount (10 sccm) and a deposition length of 35 min. From Figure 2, this thin film is 1.34 μm thick. Coating 3 is another sample that exhibited high bacterial inactivation kinetics. The slowest bacterial inactivation was seen to happen at the interface of sample 5.

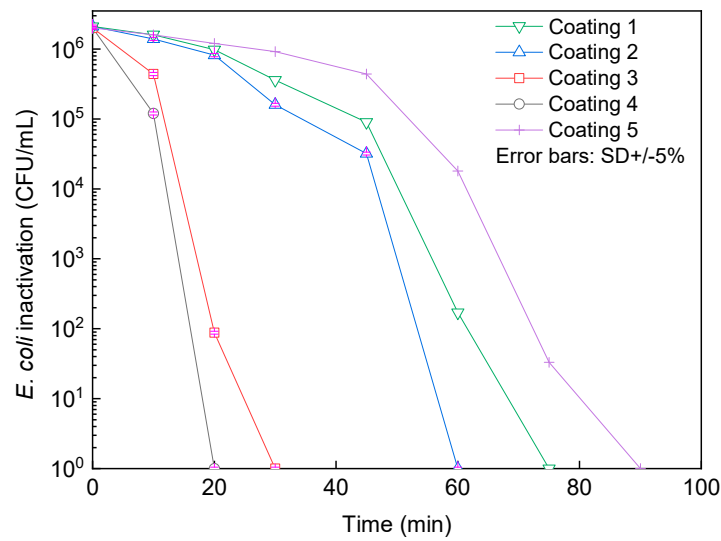


Figure 4. *E. coli* inactivation at the interface of the prepared coatings on Si wafer (coating1, coating 2, coating 3, coating 4 and coating 5).

To understand the bacterial inactivation behavior in Figure 4, the distributions of copper and oxygen atoms in the sputtered thin films were mapped by using the EDX technique, and these are shown in Figure 5 for coating 3, coating 4 and coating 5. Coatings 1 and 2 were not imaged because their bacterial inactivation kinetics were not that fast, and coating 5 was imaged for comparison purposes. It can be noticed that there is a homogeneous distribution of Cu and O along the three different coatings. Coating 3 presents 83.5% copper and 16.5% oxygen, coating 4 presents a higher oxygen content (25.8%), while coating 5 presents a lower amount (7.8%), which justifies the yellowish appearance shown in Figure 5.

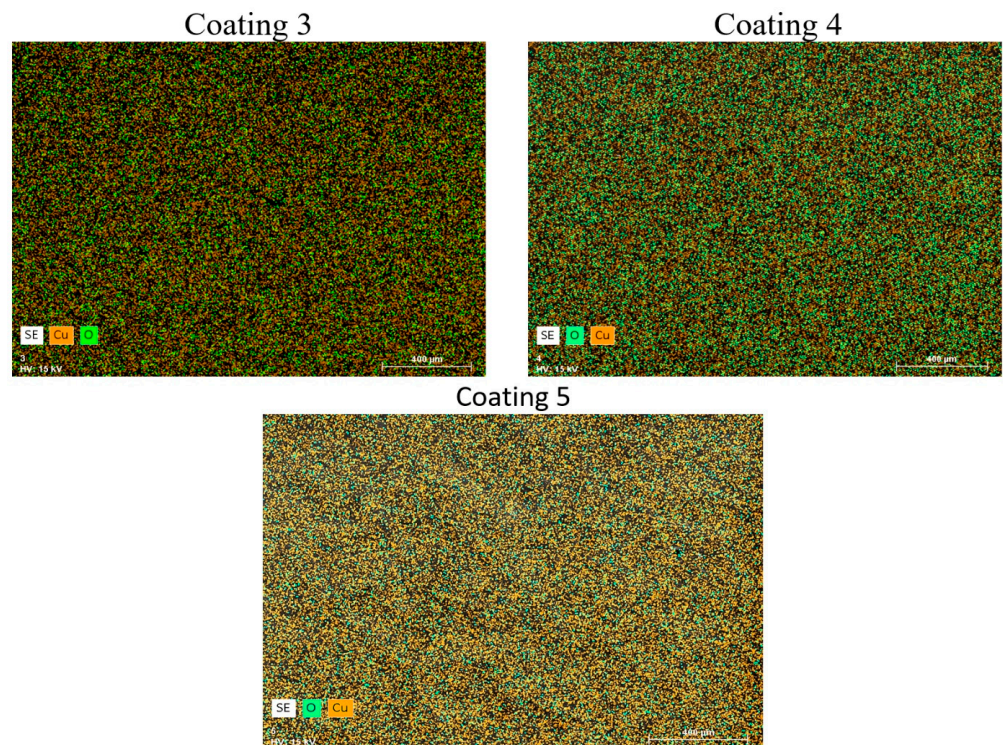


Figure 5. Distribution of copper and oxygen in the deposited films (3, 4 and 5).

3.3. Bacterial Adhesion and Inactivation at the Interface of the Prepared Surfaces

Bacterial adhesion is the first step in the interaction between a fomite surface and pathogens. However, bacterial adhesion can be affected by different parameters of the surface such as the materials' chemistry, the interface potential (*Eigenvalues*), the hydrophilicity and the roughness. Figure 6a shows the bacterial adhesion on the untreated stainless steel (SS), the polished SS, the minimally and highly SMATed samples and the sandblasted samples.

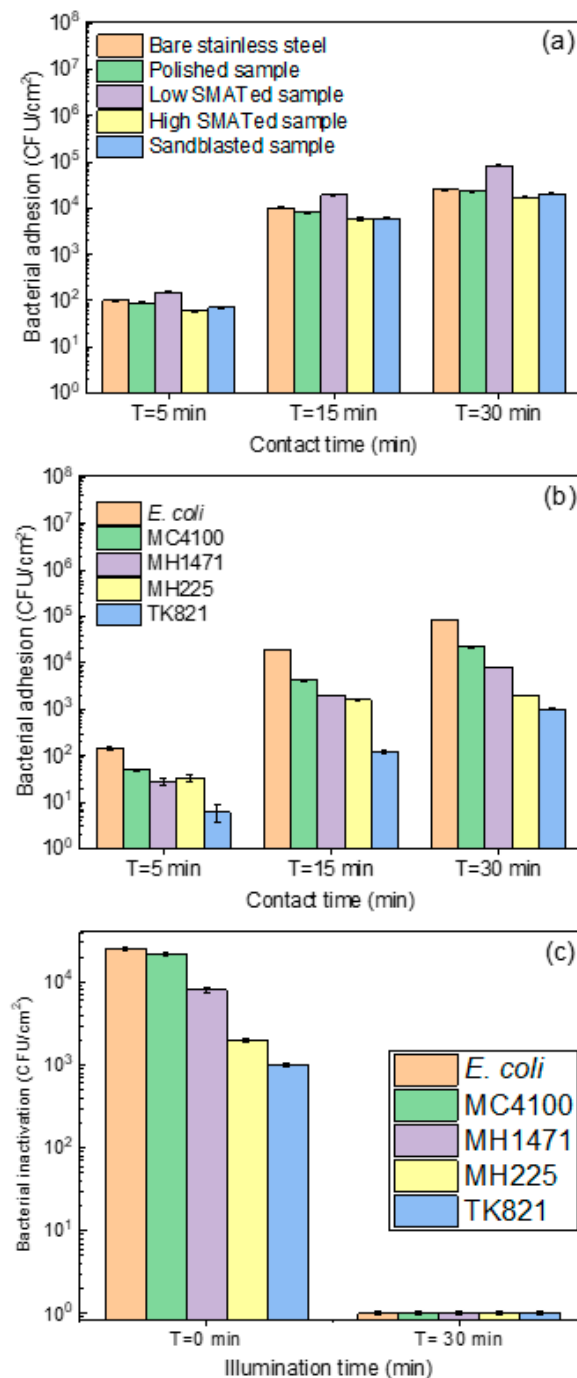


Figure 6. (a). Wild *E. coli* adsorption at the interface of bare stainless steel, polished stainless steel, low-energy SMAT stainless steel, high-energy SMAT stainless steel, and sandblasting stainless steel. (b). Different *E. coli* strains adsorption on low-energy SMAT stainless steel. (c). Inactivation of different strains of *E. coli* at the interface of low-energy SMAT stainless steel under indoor light for 30 min.

Figure 6a shows a similar tendency in bacterial adhesion, with a slightly higher adhesion on the SMATed sample at a low energy. From the roughness profiles shown in Figure 1 and Supplementary Figures S1–S4, the minimally SMATed samples presented a higher amount/number of peaks and valleys compared to those of the other prepared surfaces. This roughness profile seems the most favorable for bacterial adhesion before their inactivation under indoor light on the thin copper layer. Samples incubated with bacteria for 60 min (data not shown) showed a similar tendency to those that were incubated for 30 min. This adsorption stability can be explained by (i) the occupation of all possible valleys available on the surface or (ii) bacterial inactivation mediating the released copper ions from the sputtered surface. The molecular terminations and polar groups at the outer side of these pores are expected to control bacterial adsorption at the interface of the samples. A deeper investigation is needed to understand the molecular mechanisms allowing this bacterial adsorption, which is beyond the scope of the actual study.

Figure 6b shows the adsorption of different bacterial strains on the low-energy SMAT samples. The difference between the bacterial strains used in this experiment is mainly based on the presence/absence of OmpF and OmpC, as illustrated in Table 2. The highly studied OmpF proteins are formed of 340 amino acids. They form voltage-gated channels that span the outer membrane. OmpF (with dimensions of $7 \times 11 \text{ \AA}$) allows the diffusion of small polar molecules of $<600 \text{ Da}$, preferably positively charged entities [31]. Kefala et al. revisited the configuration of OmpF and described it as eight short β -hairpins on the periplasmic side and eight long irregular loops (L1–L8) on the extracellular side connect the antiparallel β -strands [32].

After the adsorption of the bacterial cells, their inactivation can happen under light (photocatalytic pathway) or in the dark (catalytic pathway). Figure 6c shows the bacterial inactivation under light after the adsorption phase for 30 min. Within 30 min, all bacterial strains (with or without porins) were inactivated. This highlights the aggressive effect of the photogenerated reactive oxygen species (ROS) attacking the outer cell wall. Rtimi et al. studied the contribution of the released Ag and Cu ions on bacterial inactivation compared to the extracellular bacterial inactivation process [33]. Moreover, genetically modified *E. coli* TK821 were employed to study the drastic effect of the ROS during extracellular bacterial attack [24]. The mechanism of ROS generation at the interface of sputtered Cu_xO has been previously studied [29,34]. In this study, we focused on the surface roughness contribution to bacterial adhesion and their inactivation under light afterward.

3.4. Live/Dead Bacterial Cells at the Interface of the Prepared Surfaces and Ions Release

Figure 7 shows the live/dead *E. coli* cells at the interface of low-energy SMAT stainless steel coated with a copper oxide sputtered layer. The green dots represent the live cells, and the red dots represent the dead cells. As it can be seen from Figure 7, the live bacteria were seen within the first 30 min in the dark, allowing adhesion to the surface and confirming the results shown in Figure 6a. After 30 min of illumination, all the adhered cells were practically dead for the wild *E. coli* strain. Concerning the TK821 strain, after illumination, very few (insignificant) cells were alive (in the green color) at the interface of the low-energy SMAT sample. As these bacteria did not appear when we performed the plate count agar method, they can be viable, non-cultivable cells. This means that these bacteria underwent enough cell wall injuries that did not allow them to replicate and form colonies [26,35].

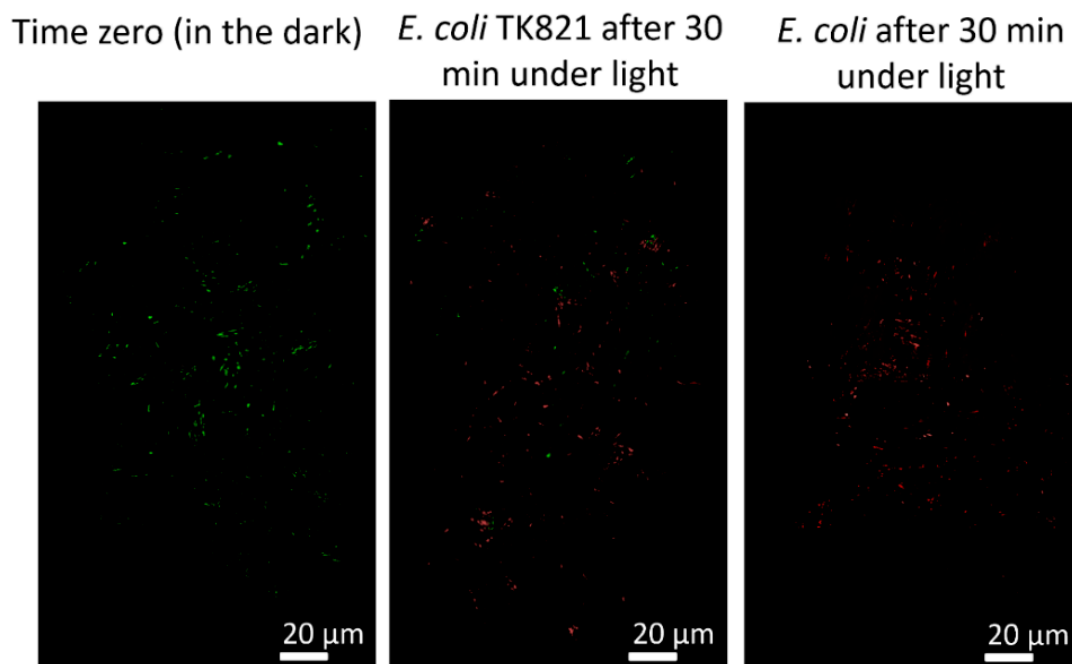


Figure 7. Live/dead bacteria images, showing the wild bacteria (presenting normal cell wall porins) and the porin-less bacteria (presenting $OmpF^-/OmpC^-$) after 30 min under indoor light at the interface low-energy SMAT stainless steel coated with a copper oxide sputtered layer.

The quantification of the Cu ions released from the low-energy SMAT surface showed values lower than 90 ppb ($\mu\text{g/L}$). Considering that $1 \text{ ppb } (w/v) = 10^{-9} \text{ g/mL} = 10^{-6} \text{ g/L}$, to convert the found amount of copper in ppb units to M, we divide the above value by the molecular weight (MW) in g/mol. Then, $90 \text{ ppb } (w/v) = 90 \times 10^{-6} / \text{Molecular Weight}$ (as the quantified copper content can only be ionic, we assume both of the ionic forms are present, namely Cu(I) and Cu(II), with molecular weights of 79.545 and 143.09 g/mol, respectively, and we then assume that $90 \times 10^{-6} \text{ g/L}$ corresponds to $0.404 \mu\text{mol/L}$). It is important to clarify that these released concentrations are found on a surface of 5 cm^2 during one bacterial inactivation cycle. It has been reported before that samples prepared by magnetron sputtering release very low amounts of the sputtered entities (in the ppb range) depending on the used deposition mode (DCMS or HiPIMS) [6,24,36,37].

This low amount of released ions was able to disturb the molecular distribution of copper around the cell wall membrane. This effect was described previously by Rtimi et al. as the oligodynamic effect affecting bacterial survival [36], although copper is a required trace element for the growth of microorganisms since it is a cofactor for numerous enzymes. However, at elevated concentrations, copper can be highly toxic to microorganisms, which is the case in this study. Nevertheless, the copper content of the commercial microbiological media shows a substantial difference. Oxoid Nutrient Broth presents $8 \mu\text{g Cu}^{2+} / \text{g}$, while only $3 \mu\text{g/g}$ is found in Difco Nutrient Broth.

At this level, we should also mention that by comparing both bacterial inactivation pathways investigated in this study, the extracellular bacterial inactivation seemed to be faster and more efficient in terms of bacterial inhibition of regrowth. Figure 8a,b shows the schematic mechanism of bacterial inactivation through cell wall attack and/or ions diffusion.

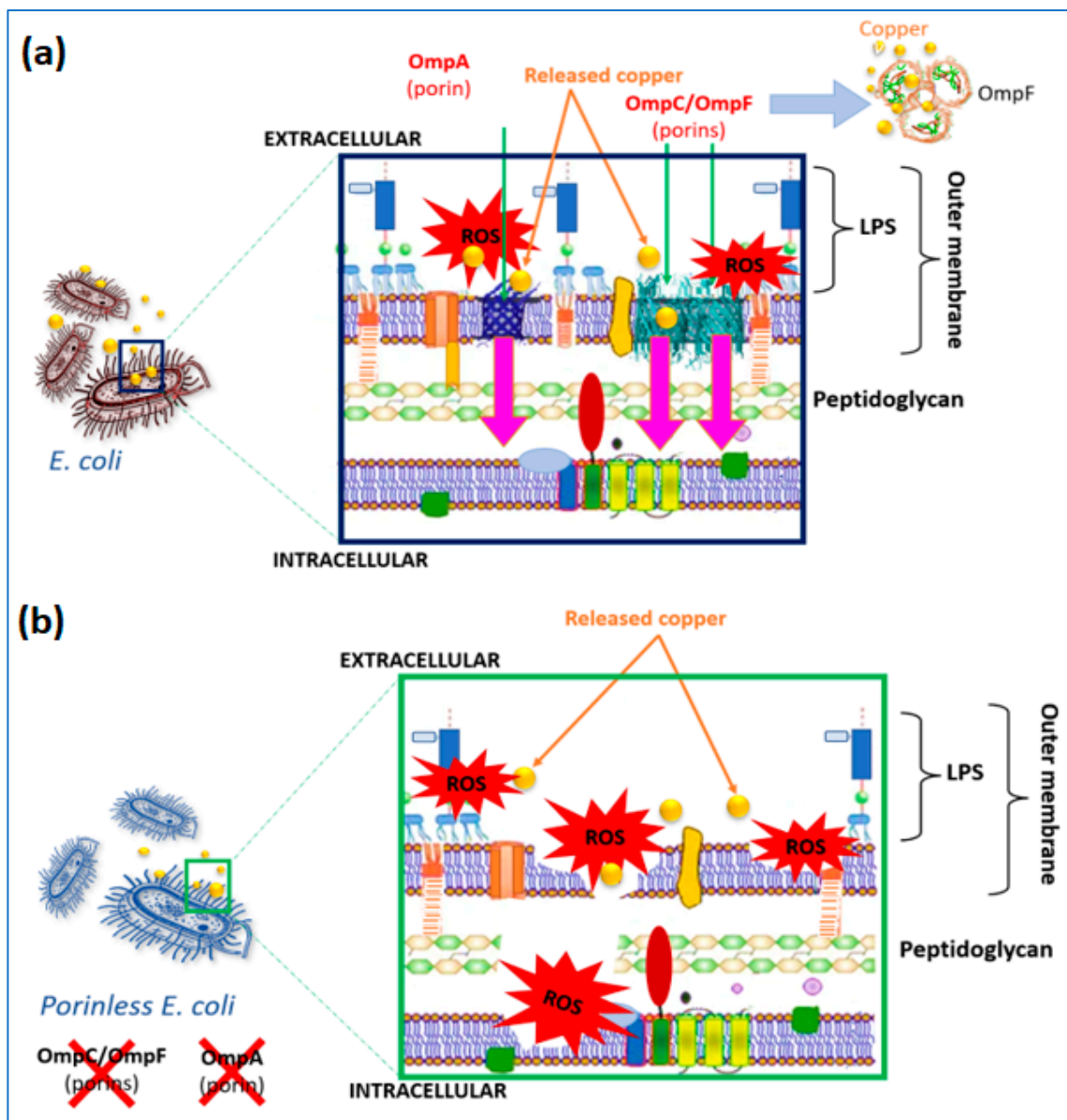


Figure 8. (a). ROS attack to cell wall membrane concomitant with ions diffusion leading to bacterial inactivation. (b). ROS attack to the cell wall of porinless bacteria: extracellular bacterial inactivation mechanism.

4. Conclusions

In this study, we prepared textured stainless-steel substrates using mirror polishing, sandblasting and Surface Mechanical Attrition Treatments (SMAT) with low and high intensities. The samples were, afterward, coated with copper oxide thin films using magnetron sputtering. The prepared samples were tested for bacterial adhesion in the dark and under low-intensity indoor light. Wild *E. coli* showed from 3 to 4Log adhered cells within 30 min of contact, and the adhered bacteria were inactivated under light within 30 min. To understand the mechanism of bacterial inactivation, whether it was due to oxidative stress at the interface of the copper oxide thin film or to the leached copper ions, we used genetically modified bacteria lacking the major pores allowing the penetration of copper to the intracellular compartment. The major porins targeted by the genetic modification were OmpC and OmpF. We also showed that the very small amount of copper ions released from the prepared surfaces (~ 20 ppb/cm²) disturbs the molecular distribution

of copper around the cell wall membrane. This work is a step closer to designing coated surfaces for public use under sustainable light sources.

Supplementary Materials: The following supporting information can be downloaded at: <https://www.mdpi.com/article/10.3390/coatings13020454/s1>, Figure S1: Analysis of surface roughness of polished reference sample; Figure S2: Analysis of surface roughness of Low SMATed reference sample; Figure S3: Analysis of surface roughness of High SMATed reference sample; Figure S4: Analysis of surface roughness of sandblasted reference sample.

Author Contributions: Conceptualization, A.A., D.R. and S.R.; methodology, A.A. and D.R.; software, L.A.; validation, A.A., D.R. and A.H.; formal analysis, L.A.; investigation, A.A., D.R., L.A. and S.R.; resources, A.A., S.R. and D.R.; data curation, A.A.; writing—original draft preparation, A.A. and L.A.; writing—review and editing, D.R. and S.R.; visualization, S.R.; supervision, S.R.; project administration, S.R.; funding acquisition, A.A. and D.R. All authors have read and agreed to the published version of the manuscript.

Funding: This research received no external funding.

Institutional Review Board Statement: Not applicable.

Informed Consent Statement: Not applicable.

Data Availability Statement: Data is available for significant request.

Acknowledgments: S. Rtimi thanks EPFL and UOC.

Conflicts of Interest: The authors declare no conflict of interest.

References

1. De Pasquale, I.; Porto, C.L.; Dell'Edera, M.; Curri, M.; Comparelli, R. TiO₂-based nanomaterials assisted photocatalytic treatment for virus inactivation: Perspectives and applications. *Curr. Opin. Chem. Eng.* **2021**, *34*, 100716. [[CrossRef](#)] [[PubMed](#)]
2. Park, H.; Bentría, E.; Rtimi, S.; Arredouani, A.; Bensmail, H.; El-Mellouhi, F. Accelerating the Design of Photocatalytic Surfaces for Antimicrobial Application: Machine Learning Based on a Sparse Dataset. *Catalysts* **2021**, *11*, 1001. [[CrossRef](#)]
3. Radetić, M.; Marković, D. A review on the role of plasma technology in the nano-finishing of textile materials with metal and metal oxide nanoparticles. *Plasma Process. Polym.* **2022**, *19*, 2100197. [[CrossRef](#)]
4. Hegemann, D.; Hanselmann, B.; Zuber, F.; Pan, F.; Gaiser, S.; Rupper, P.; Maniura-Weber, K.; Ruffieux, K.; Ren, Q. Plasma-deposited AgOx-doped TiOx coatings enable rapid antibacterial activity based on ROS generation. *Plasma Process. Polym.* **2022**, *19*, 2100246. [[CrossRef](#)]
5. Liu, S.; Zhang, S.; Yang, L.; Yu, Y.; Wang, S.; Li, L.; Wang, N.; Chen, S.; Ma, J.; Li, J. Nanofibrous scaffold by cleaner magnetron-sputtering additive manufacturing: A novel biocompatible platform for antibacterial application. *J. Clean. Prod.* **2021**, *315*, 128201. [[CrossRef](#)]
6. Rtimi, S.; Sanjines, R.; Pulgarin, C.; Kiwi, J. Microstructure of Cu-Ag Uniform Nanoparticulate Films on Polyurethane 3D Catheters: Surface Properties. *ACS Appl. Mater. Interfaces* **2016**, *8*, 56–63. [[CrossRef](#)]
7. Birkett, M.; Dover, L.; Lukose, C.C.; Zia, A.; Tambuwala, M.; Serrano-Aroca, Á. Recent Advances in Metal-Based Antimicrobial Coatings for High-Touch Surfaces. *Int. J. Mol. Sci.* **2022**, *23*, 1162. [[CrossRef](#)]
8. Govind, V.; Bharadwaj, S.; Ganesh, M.R.S.; Vishnu, J.; Shankar, K.; Shankar, B.; Rajesh, R. Antiviral properties of copper and its alloys to inactivate COVID-19 virus: A review. *BioMetals* **2021**, *34*, 1217–1235. [[CrossRef](#)]
9. Behzadinasab, S.; Chin, A.; Hosseini, M.; Poon, L.; Ducker, W. A Surface Coating that Rapidly Inactivates SARS-CoV-2. *ACS Appl. Mater. Interfaces* **2020**, *12*, 34723–34727. [[CrossRef](#)]
10. Alavi, M.; Moradi, M. Different antibacterial and photocatalyst functions for herbal and bacterial synthesized silver and copper/copper oxide nanoparticles/nanocomposites: A review. *Inorg. Chem. Commun.* **2022**, *142*, 109590. [[CrossRef](#)]
11. Bondarenko, O.; Juganson, K.; Ivsak, A.; Kasemets, M.; Mortimer, M.; Kahru, A. Toxicity of Ag, CuO and ZnO nanoparticles to selected environmentally relevant test organisms and mammalian cells in vitro: A critical review. *Arch. Toxicol.* **2013**, *87*, 1181–1200. [[CrossRef](#)] [[PubMed](#)]
12. Román, L.; Gomez, E.D.; Solís, J.L.; Gómez, M.M. Antibacterial Cotton Fabric Functionalized with Copper Oxide Nanoparticles. *Molecules* **2020**, *25*, 5802. [[CrossRef](#)] [[PubMed](#)]
13. Rigo, A.; Corazza, A.; di Paolo, M.; Rossetto, M.; Ugolini, R.; Scarpa, M. Interaction of copper with cysteine: Stability of cuprous complexes and catalytic role of cupric ions in anaerobic thiol oxidation. *J. Inorg. Biochem.* **2004**, *98*, 1495–1501. [[CrossRef](#)] [[PubMed](#)]
14. Baghriche, O.; Pulgarin, C.; Kiwi, J. Polystyrene CuO/Cu₂O uniform films inducing MB-degradation under sunlight. *Catal. Today* **2017**, *284*, 77–83. [[CrossRef](#)]
15. Parra-Ortiz, E.; Malmsten, M. Photocatalytic nanoparticles—From membrane interactions to antimicrobial and antiviral effects. *Adv. Colloid Interface Sci.* **2022**, *299*, 102526. [[CrossRef](#)]

16. Ballo, M.; Rtimi, S.; Kiwi, J.; Pulgarin, C.; Entenza, J.; Bizzini, A. Fungicidal activity of copper-sputtered flexible surfaces under dark and actinic light against azole-resistant *Candida albicans* and *Candida glabrata*. *J. Photochem. Photobiol. B Biol.* **2017**, *174*, 229–234. [CrossRef]
17. Hajjaji, A.; Elabidi, M.; Trabelsi, K.; Assadi, A.; Bessais, B.; Rtimi, S. Bacterial adhesion and inactivation on Ag decorated TiO₂-nanotubes under visible light: Effect of the nanotubes geometry on the photocatalytic activity. *Colloids Surf. B Biointerfaces* **2018**, *170*, 92–98. [CrossRef]
18. Perera-Costa, D.; Bruque, J.M.; Gonzalez-Martín, M.; Gomez-García, A.C.; Vadillo-Rodríguez, V. Studying the Influence of Surface Topography on Bacterial Adhesion using Spatially Organized Microtopographic Surface Patterns. *Langmuir* **2014**, *30*, 4633–4641. [CrossRef]
19. Senthilraj, H.; Kamarajan, B.P.; Ananthasubramanian, M. Study of bacterial attachment on the rough surfaces. *Int. J. Mech. Eng.* **2021**, *6*, 629–633.
20. Available online: <https://www.bruker.com/en/products-and-solutions/elemental-analyzers/eds-wds-ebstd-SEM-Micro-XRF/software-esprit-family/esprit-spectrum.html> (accessed on 18 October 2019).
21. Seddiki, O.; Harnagea, C.; Levesque, I.; Mantovani, D.; Rosei, F. Evidence of antibacterial activity on titanium surfaces through nanotextures. *Appl. Surf. Sci.* **2014**, *308*, 275–284. [CrossRef]
22. Kadlec, R.; Jakubec, M.; Jaglic, Z. A novel flotation technique for the separation of non-adherent microorganisms from a substrate. *Lett. Appl. Microbiol.* **2014**, *58*, 604–609. [CrossRef] [PubMed]
23. Radzig, M.; Nadtochenko, V.; Koksharova, O.; Kiwi, J.; Lipasova, V.; Khmel, I. Antibacterial effects of silver nanoparticles on gram-negative bacteria: Influence on the growth and biofilms formation, mechanisms of action. *Colloids Surf. B Biointerfaces* **2013**, *102*, 300–306. [CrossRef] [PubMed]
24. Rtimi, S.; Konstantinidis, S.; Britun, N.; Bensimon, M.; Khmel, I.; Nadtochenko, V. Extracellular bacterial inactivation proceeding without Cu-ion release: Drastic effects of the applied plasma energy on the performance of the Cu-polyester (PES) samples. *Appl. Catal. B Environ.* **2018**, *239*, 245–253. [CrossRef]
25. Forst, S.; Comeau, D.; Norioka, S.; Inouye, M. Localization and Membrane Topology of EnvZ, a Protein Involved in Osmoregulation of OmpF and OmpC in *Escherichia coli*. *J. Biol. Chem.* **1987**, *262*, 16433–16438. [CrossRef]
26. Bouabibsa, I.; Alhussein, A.; Lamri, S.; Sanchette, F.; Rtimi, S. Biological responses at the interface of Ti-doped diamond-like carbon surfaces for indoor environment application. *Environ. Sci. Pollut. Res.* **2020**, *27*, 31120–31129. [CrossRef]
27. Shin, J.W.; Lee, J.Y.; Kim, T.W.; Cho, W.J.; Choi, W.K. Growth mechanisms of thin-film columnar structures in zinc oxide on p-type silicon substrates. *Appl. Phys. Lett.* **2006**, *88*, 091911.
28. Chandra, R.; Taneja, P.; Ayyub, P. Optical properties of transparent nanocrystalline Cu₂O thin films synthesized by high pressure gas sputtering. *Nanostruct. Mater.* **1999**, *11*, 505–512. [CrossRef]
29. Rtimi, S.; Kiwi, J. Recent advances on sputtered films with Cu in ppm concentrations leading to an acceleration of the bacterial inactivation. *Catal. Today* **2020**, *340*, 347–362. [CrossRef]
30. Su, J.; Liu, Y.; Jiang, M.; Zhu, X. Oxidation of copper during physical sputtering deposition: Mechanism, avoidance and utilization. *arXiv* **2014**, arXiv:1412.2031.
31. Cowan, S.; Schirmer, T.; Rummel, G.; Steiert, M.; Ghosh, R.; Paupit, R.; Jansonius, J.; Rosenbusch, J. Crystal structures explain functional properties of two *Escherichia coli* porins. *Nature* **1992**, *358*, 727–733. [CrossRef]
32. Kefala, G.; Ahn, C.; Krupa, M.; Esquivies, L.; Maslennikov, I.; Kwiatkowski, W.; Choe, S. Structures of the OmpF porin crystallized in the presence of foscholine-12. *Protein Sci.* **2010**, *19*, 1117–1125. [CrossRef] [PubMed]
33. Rtimi, S.; Nadtochenko, V.; Khmel, I.; Bensimon, M.; Kiwi, J. First unambiguous evidence for distinct ionic and surface-contact effects during photocatalytic bacterial inactivation on Cu–Ag films: Kinetics, mechanism and energetics. *Mater. Today Chem.* **2017**, *6*, 62–74. [CrossRef]
34. Basnet, P.; Zhao, Y. Tuning the CuxO nanorod composition for efficient visible light induced photocatalysis. *Catal. Sci. Technol.* **2016**, *6*, 2228–2238. [CrossRef]
35. Chang, T.; Babu, R.P.; Zhao, W.; Johnson, C.M.; Hedström, P.; Odnevall, I.; Leygraf, C. High-Resolution Microscopical Studies of Contact Killing Mechanisms on Copper-Based Surfaces. *ACS Appl. Mater. Interfaces* **2021**, *13*, 49402–49413. [CrossRef] [PubMed]
36. Rtimi, S.; Pascu, M.; Sanjines, R.; Lavanchy, J.-C.; Kiwi, J. ZrNO-Ag co-sputtered surfaces leading to *E. coli* inactivation under actinic light: Evidence for the oligodynamic effect. *Appl. Catal. B Environ.* **2013**, *138–139*, 113–121. [CrossRef]
37. Aissani, L.; Alhussein, A.; Zia, A.W.; Mamba, G.; Rtimi, S. Magnetron Sputtering of Transition Metal Nitride Thin Films for Environmental Remediation. *Coatings* **2022**, *12*, 1746. [CrossRef]

Disclaimer/Publisher’s Note: The statements, opinions and data contained in all publications are solely those of the individual author(s) and contributor(s) and not of MDPI and/or the editor(s). MDPI and/or the editor(s) disclaim responsibility for any injury to people or property resulting from any ideas, methods, instructions or products referred to in the content.